

Determination of $|V_{cb}|$ from the semileptonic decay

$$B^0 \rightarrow D^{*-} \ell^+ \nu$$

DELPHI Collaboration

P.Abreu²¹, W.Adam⁵⁰, T.Adye³⁷, E.Agasi³¹, I.Ajinenko⁴², R.Aleksan³⁹, G.D.Alekseev¹⁶, R.Aleman⁴⁹, P.P.Allport²², S.Almehed²⁴, U.Amaldi⁹, S.Amato⁴⁷, A.Andreazza²⁸, M.L.Andrieux¹⁴, P.Antilogus⁹, W-D.Apel¹⁷, Y.Arnoud³⁹, B.Åsman⁴⁴, J-E.Augustin²⁵, A.Augustinus⁹, P.Baillon⁹, P.Bambade¹⁹, F.Barao²¹, R.Barate¹⁴, M.Barbi⁴⁷, G.Barbiellini⁴⁶, D.Y.Bardin¹⁶, A.Baroncelli⁴⁰, O.Barring²⁴, J.A.Barrio²⁶, W.Bartl⁵⁰, M.J.Bates³⁷, M.Battaglia¹⁵, M.Baubillier²³, J.Baudot³⁹, K-H.Becks⁵², M.Begalli⁶, P.Beilliere⁸, Yu.Belokopytov^{9,*}, A.C.Benvenuti⁵, M.Berggren⁴⁷, D.Bertrand², F.Bianchi⁴⁵, M.Bigi⁴⁵, M.S.Bilenky¹⁶, P.Billoir²³, D.Bloch¹⁰, M.Blume⁵², S.Blyth³⁵, T.Bolognese³⁹, M.Bonesini²⁸, W.Bonivento²⁸, P.S.L.Booth²², G.Borisov⁴², C.Bosio⁴⁰, S.Bosworth³⁵, O.Botner⁴⁸, E.Boudinov³¹, B.Bouquet¹⁹, C.Bourdarios⁹, T.J.V.Bowcock²², M.Bozzo¹³, P.Branchini⁴⁰, K.D.Brand³⁶, T.Brenke⁵², R.A.Brenner¹⁵, C.Bricman², L.Brillault²³, R.C.A.Brown⁹, P.Bruckman¹⁸, J-M.Brunet⁸, L.Bugge³³, T.Buran³³, T.Burgsmueller⁵², P.Buschmann⁵², A.Buys⁹, S.Cabrera⁴⁹, M.Caccia²⁸, M.Calvi²⁸, A.J.Camacho Rozas⁴¹, T.Camporesi⁹, V.Canale³⁸, M.Canepa¹³, K.Cankocak⁴⁴, F.Cao², F.Carena⁹, L.Carroll²², C.Caso¹³, M.V.Castillo Gimenez⁴⁹, A.Cattai⁹, F.R.Cavallo⁵, L.Cerrito³⁸, V.Chabaud⁹, M.Chapkin⁴², Ph.Charpentier⁹, L.Chaussard²⁵, J.Chauveau²³, P.Checchia³⁶, G.A.Chelkov¹⁶, M.Chen², R.Chierici⁴⁵, P.Chliapnikov⁴², P.Chochula⁷, V.Chorowicz⁹, J.Chudoba³⁰, V.Cindro⁴³, P.Collins⁹, J.L.Contreras¹⁹, R.Contri¹³, E.Cortina⁴⁹, G.Cosme¹⁹, F.Cossutti⁴⁶, H.B.Crawley¹, D.Crennell³⁷, G.Crosetti¹³, J.Cuevas Maestro³⁴, S.Czellar¹⁵, E.Dahl-Jensen²⁹, J.Dahm⁵², B.Dalmagne¹⁹, M.Dam²⁹, G.Damgaard²⁹, P.D.Dauncey³⁷, M.Davenport⁹, W.Da Silva²³, C.Defoix⁸, A.Deghorain², G.Della Ricca⁴⁶, P.Delpierre²⁷, N.Demaria³⁵, A.De Angelis⁹, W.De Boer¹⁷, S.De Brabandere², C.De Clercq², C.De La Vaissiere²³, B.De Lotto⁴⁶, A.De Min³⁶, L.De Paula⁴⁷, C.De Saint-Jean³⁹, H.Dijkstra⁹, L.Di Ciaccio³⁸, F.Djama¹⁰, J.Dolbeau⁸, M.Donszelmann⁹, K.Doroba⁵¹, M.Dracos¹⁰, J.Drees⁵², K.-A.Drees⁵², M.Dris³², Y.Dufour⁹, D.Edsall¹, R.Ehret¹⁷, G.Eigen⁴, T.Ekelof⁴⁸, G.Ekspong⁴⁴, M.Elsing⁵², J-P.Engel¹⁰, N.Ershaidat²³, B.Erzen⁴³, M.Espirito Santo²¹, E.Falk²⁴, D.Fassouliotis³², M.Feindt⁹, A.Fenyuk⁴², A.Ferrer⁴⁹, T.A.Filippas³², A.Firestone¹, P.-A.Fischer¹⁰, H.Foeth⁹, E.Fokitis³², F.Fontanelli¹³, F.Formenti⁹, B.Franek³⁷, P.Frenkiel⁸, D.C.Fries¹⁷, A.G.Frodesen⁴, R.Fruhworth⁵⁰, F.Fulda-Quenzer¹⁹, J.Fuster⁴⁹, A.Galloni²², D.Gamba⁴⁵, M.Gandelman⁶, C.Garcia⁴⁹, J.Garcia⁴¹, C.Gaspar⁹, U.Gasparini³⁶, Ph.Gavillet⁹, E.N.Gazizade³², D.Gele¹⁰, J-P.Gerber¹⁰, M.Gibbs²², R.Gokieli⁵¹, B.Golob⁴³, G.Gopal³⁷, L.Gorn¹, M.Gorski⁵¹, Yu.Gouz^{45,*}, V.Gracco¹³, E.Graziani⁴⁰, G.Grosdidier¹⁹, K.Grzelak⁵¹, S.Gumenyuk^{28,*}, P.Gunnarsson⁴⁴, M.Gunther⁴⁸, J.Guy³⁷, F.Hahn⁹, S.Hahn⁵², Z.Hajduk¹⁸, A.Hallgren⁴⁸, K.Hamacher⁵², W.Hao³¹, F.J.Harris³⁵, V.Hedberg²⁴, R.Henriques²¹, J.J.Hernandez⁴⁹, P.Herquet², H.Herr⁹, T.L.Hessing³⁵, E.Higon⁴⁹, H.J.Hilke⁹, T.S.Hill¹, S-O.Holmgren⁴⁴, P.J.Holt³⁵, D.Holthuisen³¹, S.Hoorelbeke², M.Houlden²², J.Hrubec⁵⁰, K.Huet², K.Hultqvist⁴⁴, J.N.Jackson²², R.Jacobsson⁴⁴, P.Jalocha¹⁸, R.Janik⁷, Ch.Jarlskog²⁴, G.Jarlskog²⁴, P.Jarry³⁹, B.Jean-Marie¹⁹, E.K.Johansson⁴⁴, L.Jonsson²⁴, P.Jonsson²⁴, C.Joram⁹, P.Juillot¹⁰, M.Kaiser¹⁷, F.Kapusta²³, K.Karafasoulis¹¹, M.Karlsson⁴⁴, E.Karvelas¹¹, S.Katsanevas³, E.C.Katsoufis³², R.Keranen⁴, Yu.Khokhlov⁴², B.A.Khomenko¹⁶, N.N.Khovanski¹⁶, B.King²², N.J.Kjaer²⁹, H.Klein⁹, A.Klovning⁴, P.Kluit³¹, B.Koene³¹, P.Kokkinias¹¹, M.Koratzinos⁹, K.Korcyl¹⁸, C.Kourkoumelis³, O.Kouznetsov^{13,16}, P.-H.Kramer⁵², M.Krammer⁵⁰, C.Kreuter¹⁷, I.Kronkvist²⁴, Z.Krumstein¹⁶, W.Krupinski¹⁸, P.Kubinec⁷, W.Kucewicz¹⁸, K.Kurvinen¹⁵, C.Lacasta⁴⁹, I.Laktineh²⁵, S.Lamblot²³, J.W.Lamsa¹, L.Lanceri⁴⁶, D.W.Lane¹, P.Langefeld⁵², I.Last²², J-P.Laugier³⁹, R.Lauhakangas¹⁵, G.Leder⁵⁰, F.Ledroit¹⁴, V.Lefebure², C.K.Legan¹, R.Leitner³⁰, Y.Lemoigne³⁹, J.Lemonne², G.Lenzen⁵², V.Lepeltier¹⁹, T.Lesiak³⁶, D.Liko⁵⁰, R.Lindner⁵², A.Lipniacka³⁶, I.Lippi³⁶, B.Loerstad²⁴, J.G.Loken³⁵, J.M.Lopez⁴¹, D.Loukas¹¹, P.Lutz³⁹, L.Lyons³⁵, G.Maehlum¹⁷, A.Maio²¹, V.Malychev¹⁶, F.Mandl⁵⁰, J.Marco⁴¹, R.Marco⁴¹, B.Marechal⁴⁷, M.Margoni³⁶, J-C.Marin⁹, C.Mariotti⁴⁰, A.Markou¹¹, T.Maron⁵², C.Martinez-Rivero⁴¹, F.Martinez-Vidal⁴⁹, S.Marti i Garcia⁴⁹, J.Masik³⁰, F.Matorras⁴¹, C.Matteuzzi⁹, G.Matthiae³⁸, M.Mazzucato³⁶, M.Mc Cubbin⁹, R.Mc Kay¹, R.Mc Nulty²², J.Medbo⁴⁸, M.Merk³¹, C.Meroni²⁸, S.Meyer¹⁷, W.T.Meyer¹, M.Michelotto³⁶, E.Migliore⁴⁵, L.Mirabito²⁵, W.A.Mitaroff⁵⁰, U.Mjoernmark²⁴, T.Moa⁴⁴, R.Moeller²⁹, K.Moenig⁹, M.R.Monge¹³, P.Morettini¹³, H.Mueller¹⁷, L.M.Mundim⁶, W.J.Murray³⁷, B.Muryn¹⁸, G.Myatt³⁵, F.Naraghi¹⁴, F.L.Navarria⁵, S.Navas⁴⁹, K.Nawrocki⁵¹, P.Negri²⁸, S.Nemecek¹², W.Neumann⁵², N.Neumeister⁵⁰, R.Nicolaidou³, B.S.Nielsen²⁹, M.Nieuwenhuizen³¹, V.Nikolaenko¹⁰, P.Niss⁴⁴, A.Nomerotski³⁶, A.Normand³⁵, M.Novak¹², W.Oberschulte-Beckmann¹⁷, V.Obraztsov⁴², A.G.Olshevski¹⁶, A.Onofre²¹, R.Orava¹⁵, K.Osterberg¹⁵, A.Ouraou³⁹, P.Paganini¹⁹, M.Paganoni⁹, P.Pages¹⁰, H.Palka¹⁸, Th.D.Papadopoulou³², K.Papageorgiou¹¹, L.Pape⁹, C.Parkes³⁵, F.Parodi¹³, A.Passeri⁴⁰, M.Pegoraro³⁶, L.Peralta²¹, H.Pernegger⁵⁰, M.Pernicka⁵⁰, A.Perrotta⁵, C.Petridou⁴⁶, A.Petrolini¹³, M.Petrovyck^{28,*}, H.T.Phillips³⁷, G.Piana¹³, F.Pierre³⁹, M.Pimenta²¹, M.Pindo²⁸, S.Plaszczynski¹⁹, O.Podobrin¹⁷, M.E.Pol⁹, G.Polok¹⁸, P.Poropat⁴⁶, V.Pozdniakov¹⁶, M.Prest⁴⁶, P.Privitera³⁸, N.Pukhaeva¹⁶, A.Pullia²⁸, D.Radojicic³⁵, S.Ragazzi²⁸, H.Rahmani³², P.N.Ratoff²⁰, A.L.Read³³, M.Reale⁵², P.Rebecchi¹⁹, N.G.Redaeli²⁸, M.Regler⁵⁰, D.Reid⁹,

P.B.Renton³⁵, L.K.Resvanis³, F.Richard¹⁹, J.Richardson²², J.Ridky¹², G.Rinaudo⁴⁵, I.Ripp³⁹, A.Romero⁴⁵, I.Roncagliolo¹³, P.Ronchese³⁶, L.Roos¹⁴, E.I.Rosenberg¹, E.Rosso⁹, P.Roudeau¹⁹, T.Rovelli⁵, W.Ruckstuhl³¹, V.Ruhlmann-Kleider³⁹, A.Ruiz⁴¹, K.Rybicki¹⁸, H.Saarikko¹⁵, Y.Sacquin³⁹, A.Sadovsky¹⁶, G.Sajot¹⁴, J.Salt⁴⁹, J.Sanchez²⁶, M.Sannino¹³, M.Schimmelpfennig¹⁷, H.Schneider¹⁷, U.Schwickerath¹⁷, M.A.E.Schyns⁵², G.Sciolla⁴⁵, F.Scuri⁴⁶, P.Seager²⁰, Y.Sedykh¹⁶, A.M.Segar³⁵, A.Seitz¹⁷, R.Sekulin³⁷, R.C.Shellard⁶, I.Siccama³¹, P.Siegrist³⁹, S.Simonetti³⁹, F.Simonetti³⁶, A.N.Sisakian¹⁶, B.Sitar⁷, T.B.Skaali³³, G.Smadija²⁵, N.Smirnov⁴², O.Smirnova²⁴, G.R.Smith³⁷, O.Solovianov⁴², R.Sosnowski⁵¹, D.Souza-Santos⁶, T.Spaso²¹, E.Spiriti⁴⁰, P.Sponholz⁵², S.Squarcia¹³, C.Stanescu⁴⁰, S.Stapnes³³, I.Stavitski³⁶, F.Stichelbaut⁹, A.Stocchi¹⁹, J.Strauss⁵⁰, R.Strub¹⁰, B.Stugu⁴, M.Szczekowski⁵¹, M.Szeptycka⁵¹, T.Tabarelli²⁸, J.P.Tavernet²³, O.Tchikilev⁴², A.Tilquin²⁷, J.Timmermans³¹, L.G.Tkatchev¹⁶, T.Todorov¹⁰, D.Z.Toet³¹, A.Tomaradze², A.Tonazzo²⁸, L.Tortora⁴⁰, G.Transtromer²⁴, D.Treille⁹, W.Trischuk⁹, G.Tristram⁸, A.Trombini¹⁹, C.Troncon²⁸, A.Tsirou⁹, M-L.Turluer³⁹, I.A.Tyapkin¹⁶, M.Tyndel³⁷, S.Tzamaras²², B.Ueberschaer⁵², O.Ullaland⁹, V.Uvarov⁴², G.Valenti⁵, E.Vallazza⁹, C.Vander Velde², G.W.Van Apeldoorn³¹, P.Van Dam³¹, W.K.Van Doninck², J.Van Eldik³¹, N.Vassilopoulos³⁵, G.Vegni²⁸, L.Ventura³⁶, W.Venus³⁷, F.Verbeure², M.Verlato³⁶, L.S.Vertogradov¹⁶, D.Vilanova³⁹, P.Vincent²⁵, L.Vitale⁴⁶, E.Vlasov⁴², A.S.Vodopyanov¹⁶, V.Vrba¹², H.Wahlen⁵², C.Walck⁴⁴, M.Weierstall⁵², P.Weilhammer⁹, C.Weiser¹⁷, A.M.Wetherell⁹, D.Wicke⁵², J.H.Wickens², M.Wielers¹⁷, G.R.Wilkinson³⁵, W.S.C.Williams³⁵, M.Winter¹⁰, M.Witek¹⁸, K.Woschnagg⁴⁸, K.Yip³⁵, O.Yushchenko⁴², F.Zach²⁵, A.Zaitsev⁴², A.Zalewska¹⁸, P.Zalewski⁵¹, D.Zavrtanik⁴³, E.Zevgolatakos¹¹, N.I.Zimin¹⁶, M.Zito³⁹, D.Zontar⁴³, R.Zuberi³⁵, G.C.Zucchelli⁴⁴, G.Zumerle³⁶

¹ Ames Laboratory and Department of Physics, Iowa State University, Ames, IA 50011, USA

² Physics Department, Univ. Instelling Antwerpen, Universiteitsplein 1, B-2610 Wilrijk, Belgium and IIHE, ULB-VUB, Pleinlaan 2, B-1050 Brussels, Belgium and Faculté des Sciences, Univ. de l'Etat Mons, Av. Maistriau 19, B-7000 Mons, Belgium

³ Physics Laboratory, University of Athens, Solonos Str. 104, GR-10680 Athens, Greece

⁴ Department of Physics, University of Bergen, Allégaten 55, N-5007 Bergen, Norway

⁵ Dipartimento di Fisica, Università di Bologna and INFN, Via Irnerio 46, I-40126 Bologna, Italy

⁶ Centro Brasileiro de Pesquisas Físicas, rua Xavier Sigaud 150, RJ-22290 Rio de Janeiro, Brazil and Depto. de Física, Pont. Univ. Católica, C.P. 38071, RJ-22453 Rio de Janeiro, Brazil and Inst. de Física, Univ. Estadual do Rio de Janeiro, rua São Francisco Xavier 524, Rio de Janeiro, Brazil

⁷ Comenius University, Faculty of Mathematics and Physics, Mlynska Dolina, SK-84215 Bratislava, Slovakia

⁸ Collège de France, Lab. de Physique Corpusculaire, IN2P3-CNRS, F-75231 Paris Cedex 05, France

⁹ CERN, CH-1211 Geneva 23, Switzerland

¹⁰ Centre de Recherche Nucléaire, IN2P3 - CNRS/ULP - BP20, F-67037 Strasbourg Cedex, France

¹¹ Institute of Nuclear Physics, N.C.S.R. Demokritos, P.O. Box 60228, GR-15310 Athens, Greece

¹² FZU, Inst. of Physics of the C.A.S. High Energy Physics Division, Na Slovance 2, 180 40, Praha 8, Czech Republic

¹³ Dipartimento di Fisica, Università di Genova and INFN, Via Dodecaneso 33, I-16146 Genova, Italy

¹⁴ Institut des Sciences Nucléaires, IN2P3-CNRS, Université de Grenoble 1, F-38026 Grenoble Cedex, France

¹⁵ Research Institute for High Energy Physics, SEFT, P.O. Box 9, FIN-00014 Helsinki, Finland

¹⁶ Joint Institute for Nuclear Research, Dubna, Head Post Office, P.O. Box 79, 101 000 Moscow, Russia

¹⁷ Institut für Experimentelle Kernphysik, Universität Karlsruhe, Postfach 6980, D-76128 Karlsruhe, Germany

¹⁸ Institute of Nuclear Physics and University of Mining and Metallurgy, Ul. Kawiora 26a, PL-30055 Krakow, Poland

¹⁹ Université de Paris-Sud, Lab. de l'Accélérateur Linéaire, IN2P3-CNRS, Bât. 200, F-91405 Orsay Cedex, France

²⁰ School of Physics and Materials, University of Lancaster, Lancaster LA1 4YB, UK

²¹ LIP, IST, FCUL - Av. Elias Garcia, 14-1º, P-1000 Lisboa Codex, Portugal

²² Department of Physics, University of Liverpool, P.O. Box 147, Liverpool L69 3BX, UK

²³ LPNHE, IN2P3-CNRS, Universités Paris VI et VII, Tour 33 (RdC), 4 place Jussieu, F-75252 Paris Cedex 05, France

²⁴ Department of Physics, University of Lund, Sölvegatan 14, S-22363 Lund, Sweden

²⁵ Université Claude Bernard de Lyon, IPNL, IN2P3-CNRS, F-69622 Villeurbanne Cedex, France

²⁶ Universidad Complutense, Avda. Complutense s/n, E-28040 Madrid, Spain

²⁷ Univ. d'Aix - Marseille II - CPP, IN2P3-CNRS, F-13288 Marseille Cedex 09, France

²⁸ Dipartimento di Fisica, Università di Milano and INFN, Via Celoria 16, I-20133 Milano, Italy

²⁹ Niels Bohr Institute, Blegdamsvej 17, DK-2100 Copenhagen 0, Denmark

³⁰ NC, Nuclear Centre of MFF, Charles University, Areal MFF, V Holesovickach 2, 180 00, Praha 8, Czech Republic

³¹ NIKHEF-H, Postbus 41882, NL-1009 DB Amsterdam, The Netherlands

³² National Technical University, Physics Department, Zografou Campus, GR-15773 Athens, Greece

³³ Physics Department, University of Oslo, Blindern, N-1000 Oslo 3, Norway

³⁴ Dpto. Fisica, Univ. Oviedo, C/P. Pérez Casas, S/N-33006 Oviedo, Spain

³⁵ Department of Physics, University of Oxford, Keble Road, Oxford OX1 3RH, UK

³⁶ Dipartimento di Fisica, Università di Padova and INFN, Via Marzolo 8, I-35131 Padua, Italy

³⁷ Rutherford Appleton Laboratory, Chilton, Didcot OX11 0QX, UK

³⁸ Dipartimento di Fisica, Università di Roma II and INFN, Tor Vergata, I-00173 Rome, Italy

³⁹ Centre d'Etudes de Saclay, DSM/DAPNIA, F-91191 Gif-sur-Yvette Cedex, France

⁴⁰ Istituto Superiore di Sanità, Ist. Naz. di Fisica Nucl. (INFN), Viale Regina Elena 299, I-00161 Rome, Italy

⁴¹ Instituto de Fisica de Cantabria (CSIC-UC), Avda. los Castros, S/N-39006 Santander, Spain, (CICYT-AEN93-0832)

⁴² Inst. for High Energy Physics, Serpukov P.O. Box 35, Protvino, (Moscow Region), Russia

⁴³ J. Stefan Institute and Department of Physics, University of Ljubljana, Jamova 39, SI-61000 Ljubljana, Slovenia

⁴⁴ Fysikum, Stockholm University, Box 6730, S-113 85 Stockholm, Sweden

⁴⁵ Dipartimento di Fisica Sperimentale, Università di Torino and INFN, Via P. Giuria 1, I-10125 Turin, Italy

⁴⁶ Dipartimento di Fisica, Università di Trieste and INFN, Via A. Valerio 2, I-34127 Trieste, Italy and Istituto di Fisica, Università di Udine, I-33100 Udine, Italy

⁴⁷ Univ. Federal do Rio de Janeiro, C.P. 68528 Cidade Univ., Ilha do Fundão BR-21945-970 Rio de Janeiro, Brazil

⁴⁸ Department of Radiation Sciences, University of Uppsala, P.O. Box 535, S-751 21 Uppsala, Sweden

⁴⁹ IFIC, Valencia-CSIC, and D.F.A.M.N., U. de Valencia, Avda. Dr. Moliner 50, E-46100 Burjassot (Valencia), Spain

⁵⁰ Institut für Hochenergiephysik, Österr. Akad. d. Wissensch., Nikolsdorfergasse 18, A-1050 Vienna, Austria

⁵¹ Inst. Nuclear Studies and University of Warsaw, Ul. Hoza 69, PL-00681 Warsaw, Poland

⁵² Fachbereich Physik, University of Wuppertal, Postfach 100 127, D-42097 Wuppertal 1, Germany

* On leave of absence from IHEP Serpukhov

Received: 7 February 1996 / Revised version: 23 April 1996

Abstract. Semileptonic decays $B \rightarrow D^{*-} \ell^+ \nu X$ were selected from a sample of 3.1 million hadronic Z decays collected by the DELPHI detector at LEP. A topological search for semileptonic B decays to resonant and non-resonant $D^{*-} \pi^+$ states was performed and the ratio of the branching fractions:

$$\frac{Br(B \rightarrow D^{*-} \ell^+ \nu X)}{Br(B \rightarrow D^{*-} \ell^+ \nu X) + Br(B^0 \rightarrow D^{*-} \ell^+ \nu)}$$

$$= 0.19 \pm 0.10(\text{stat}) \pm 0.06(\text{syst})$$

was determined. Taking into account this contribution, the differential decay width of $B^0 \rightarrow D^{*-} \ell^+ \nu$ was measured as a function of the momentum transfer from the B to the D^{*-} in two separate analyses, using exclusive and inclusive methods of D^{*-} reconstruction. The distributions were fitted over the full momentum transfer range to extract the product of $|V_{cb}|$ times the normalization of the decay form factor $F(q_{max}^2)$:

$$F(q_{max}^2)|V_{cb}| = (35.4 \pm 1.9(\text{stat}) \pm 2.4(\text{syst})) \cdot 10^{-3}.$$

The value of $|V_{cb}|$ was computed using theoretical calculations of $F(q_{max}^2)$, giving:

$$|V_{cb}| = (38.9 \pm 2.0(\text{stat}) \pm 2.6(\text{syst}) \pm 1.7(\text{theory})) \cdot 10^{-3}.$$

The total branching fraction $Br(B^0 \rightarrow D^{*-} \ell^+ \nu)$ was determined to be:

$$Br(B^0 \rightarrow D^{*-} \ell^+ \nu) = (5.52 \pm 0.17(\text{stat}) \pm 0.68(\text{syst})\%.$$

1 Introduction

Precise measurements of the elements of the Cabibbo-Kobayashi-Maskawa matrix are required in order to complete the current picture of the weak interactions.

The magnitude of the element V_{cb} relating the beauty to the charm quark has been determined from the partial semileptonic decay width of B hadrons which is proportional to $|V_{cb}|^2$ [1]. The precision of these measurements is however limited by the understanding of the hadronisation processes involved in the decays.

The study of the properties of QCD in the infinite quark mass approximation allows the extraction of $|V_{cb}|$ with a smaller theoretical uncertainty when the semileptonic decay $B^0 \rightarrow D^{*-} \ell^+ \nu$ is considered¹. In the massless lepton limit the differential decay width, $d\Gamma/dq^2$, of this process is expressed in terms of three form factors [2], where the variable q^2 is the square of the four momentum transfer from the B^0 to the D^{*-} particle:

$$q^2 = (p_B - p_{D^*})^2.$$

¹ Throughout the paper charge-conjugate states are implicitly included. "Leptons" refers to electrons and muons

The Heavy Quark Effective Theory (HQET) [3] relates the three form factors to a single universal function, $F(q^2)$. The shape of this function is not predicted by the theory but its value at maximum momentum transfer q_{max}^2 (i.e. when the D^{*-} is produced at rest in the B frame) is normalised to 1 in the limit of infinite b and c quark masses. Corrections due to finite quark masses are computed by means of an expansion in terms of $\Lambda_{QCD}/m_{b,c}$ [4]. As a consequence of Luke's theorem [5], first order terms do not contribute and the expansion is dominated by the term proportional to $(\Lambda_{QCD}/m_c)^2$ [6]. Another theoretical uncertainty of comparable size is induced by perturbative QCD which is at present computed to first order in α_s . The measurement of the decay rate at q_{max}^2 therefore currently provides the determination of $|V_{cb}|$ with the smallest theoretical error [7].

Previous measurements of $|V_{cb}|$ based on this approach were performed by the ARGUS and CLEO collaborations at the $\Upsilon(4S)$ [2, 8, 9] and by ALEPH at LEP [10]. The relative merits of the $\Upsilon(4S)$ and LEP measurements are discussed in detail in ref.[10].

Results from two complementary analyses are reported in the present paper. The first analysis exploited events in which an exclusively reconstructed D^{*-} and a lepton were found in the same hemisphere as defined by the thrust axis. The event selection and reconstruction are described in section 4. An inclusive D^{*-} reconstruction was also performed by using events with a lepton and a slow pion in the same jet, as described in section 5. It provides higher statistics but with a higher level of background and poorer q^2 resolution.

Semileptonic decays to orbitally excited states ($D_J^{(*)}$) are predicted by HQET and have been observed recently [11]. These states provide an important source of background due to their decay into a D^{*-} plus other particles. A topological search for such states was therefore performed to determine the amount of such a background in a model-independent way. The analysis is described in section 6. The contributions from other background sources are discussed in section 7.

Due to the vanishing phase-space at q_{max}^2 the measurement is performed by extrapolating the differential decay width, $d\Gamma/dq^2$. Details of the fitting procedure are given in section 8. Systematic errors are discussed in section 9. The combined result from the two analyses is reported in section 10. Conclusions are drawn in section 11.

2 The DELPHI detector

The DELPHI detector has been described in detail elsewhere [12, 13]; only the detectors relevant to the present analysis are briefly described in the following. The tracking of charged particles is accomplished in the barrel region

with a set of cylindrical tracking detectors whose axis is oriented along the 1.23 T magnetic field and the direction of the beam. The Vertex Detector (VD) has an intrinsic resolution of 5–6 μm and consists of three concentric layers of silicon microstrip detectors at average radii of 6.3 cm, 9.0 cm, and 10.9 cm. The VD surrounds a Beryllium beam pipe with a radius of 5.6 cm. In 1991–1993 all the VD layers were single-sided with strips parallel to the beam direction. In the 1994 run the innermost and the outermost layers were replaced by double-sided silicon microstrip modules [14] giving measurements also in the direction along the beam axis (z). The Inner Detector is placed outside the VD between radii of 12 cm and 28 cm. It consists of a jet chamber giving up to 24 spatial measurements and a trigger chamber providing a measurement of the z coordinate. The VD and ID are surrounded by the main DELPHI tracking chamber, the Time Projection Chamber (TPC), which provides up to 16 space points between radii of 30 cm and 122 cm. The Outer Detector (OD) at a radius of 197 cm to 206 cm consists of five layers of drift cells. The average momentum resolution of the tracking system is $\sigma(p)/p = 0.0006 p$ (p in GeV/c) for high momentum particles, in the polar region between 30° and 150° . In the plane orthogonal to the beam direction the asymptotic precision of extrapolating tracks to the collision point was measured as $20 \pm 2 \mu\text{m}$ using muons from $Z \rightarrow \mu^+ \mu^-$ decay. In hadronic events, the extrapolation accuracy was found to be $\sqrt{20^2 + 65^2/p_t^2} \mu\text{m}$ [14] where p_t is the momentum of the particle in GeV/c in the plane transverse to the beam axis.

Electron identification relies on the electromagnetic calorimeter in the barrel region (High density Projection Chamber HPC) which is a sampling device with relative energy resolution of $\pm 6.5\%$ for electrons with $45.6 \text{ GeV}/c$ momentum, and a spatial resolution along the beam axis of $\pm 2 \text{ mm}$. The electron identification algorithm is described in ref. [13]. Within the HPC acceptance, electrons of momentum above $3 \text{ GeV}/c$ are identified with an efficiency of $\sim 77\%$. The probability of a pion being misidentified as an electron is below 1%.

The muon identification relies mainly on the muon chambers, a set of drift chambers giving three-dimensional information situated at the periphery of DELPHI after approximately 1 m of iron. The muon identification algorithm is described in ref. [13]. A loose selection criterion provided an identification efficiency of $\sim 90\%$ within the acceptance of the muon chambers for a misidentification probability of $\sim 1.3\%$ (referred to as “loose” muons in this paper). Tighter cuts gave 77% efficiency for a 0.8% misidentification probability (referred to as “standard” muons).

3 Event selection and simulation

Charged particles were required to have a measured momentum between $0.1 \text{ GeV}/c$ and $50 \text{ GeV}/c$, a relative error on momentum less than 100%, a track length larger than 30 cm and a distance of closest approach to the interaction point below 5 cm in radius and 10 cm along the beam axis. Neutral particles were required to have an energy between 1 GeV and 30 GeV and a polar angle between 20° and 160° . They were assigned the photon mass.

Hadronic events were selected using only the selected charged particles with momentum above $0.4 \text{ GeV}/c$. Five or more charged particles were required, carrying in total more than 12% of the collision energy assuming them to be pions. In total 3.1 million hadronic events were obtained from the 1991–1994 data.

Simulated hadronic events were generated using the JETSET 7.3 Parton Shower program [15]. The B meson mean lifetime was set to 1.6 ps. The generated events were followed through the detailed detector simulation DELSIM [16] and then processed through the same analysis chain as the real data. The hadronic event selection efficiency was thus estimated to be $(95.1 \pm 0.2)\%$. A total of 7 million simulated Z hadronic decays was used. To increase the statistical significance of the simulation, a special set of events was generated, each containing at least one B meson decaying to a $D^* \ell \nu$ or $D_j^{(*)} \ell \nu$ final state, corresponding to ~ 20 million hadronic Z decays.

Charged and neutral particles were clustered into jets using the LUCCLUS algorithm with default parameters [15]. For the jet containing the lepton candidate, the jet axis was defined as the sum of the momenta of all the particles in the jet except the lepton. The transverse momentum, p_T^ℓ , of the lepton with respect to this jet axis was required to exceed $0.8 \text{ GeV}/c$ in the exclusive analysis and $1 \text{ GeV}/c$ in the inclusive analysis. Furthermore, leptons with momentum greater or equal to $3 \text{ GeV}/c$ were used in the exclusive analysis; in the inclusive analysis the same cut was set at $2 \text{ GeV}/c$.

Each event was divided into two hemispheres by the plane perpendicular to the thrust axis, which was computed using all the charged and neutral particles.

4 Exclusive analysis

This section describes the exclusive reconstruction of D^* particles and the corresponding q^2 reconstruction procedure.

4.1 $D^{*-} \ell^+$ selection

The D^* candidates were reconstructed in the channel $D^{*-} \rightarrow \bar{D}^0 \pi^-$ and the \bar{D}^0 candidates were reconstructed in the decay modes $\bar{D}^0 \rightarrow K^+ \pi^-$ and $\bar{D}^0 \rightarrow K^+ \pi^- \pi^+ \pi^-$.

First, the primary interaction vertex was computed in space for each event using an iterative procedure based on the χ^2 of the vertex fit as described in ref. [17]. The primary vertex of $Z \rightarrow b\bar{b}$ events was thus evaluated with a transverse precision of about $70 \mu\text{m}$ horizontally and $30 \mu\text{m}$ vertically.

Only charged particles produced in the same jet as the lepton were considered for the reconstruction of charmed mesons. The kaon candidate in the \bar{D}^0 decay was required to have the same charge as the identified lepton.

Only particle tracks with at least one VD hit were used for the $\bar{D}^0 \rightarrow K^+ \pi^-$ channel. For the $\bar{D}^0 \rightarrow K^+ \pi^- \pi^+ \pi^-$ decay channel, at least one hit was required on at least two of the four tracks of the \bar{D}^0 candidate. After a $K^+ \pi^-$ or $K^+ \pi^- \pi^- \pi^+$ combination was selected, its vertex was computed in space and the momentum vector of each particle was

recalculated at this position. In the $\bar{D}^0 \rightarrow K^+\pi^-$ channel, the momentum of each particle had to be larger than 1 GeV/c. For $\bar{D}^0 \rightarrow K^+\pi^-\pi^+\pi^-$ decays, the minimum momentum required for candidate pions was lowered to 0.2 GeV/c. In order to select events with well reconstructed secondary vertices for $K3\pi$ candidates, the impact parameter to the secondary vertex of each decay particle was required to be less than 300 μm .

To reduce the combinatorial background in the $\bar{D}^0 \rightarrow K^+\pi^-$ channel, the angle θ^* between the \bar{D}^0 flight direction and the kaon direction in the \bar{D}^0 rest frame was required to satisfy the condition $\cos\theta^* > -0.9$. For genuine $\bar{D}^0 \rightarrow K^+\pi^-$ candidates an isotropic distribution in $\cos\theta^*$ is expected whereas the background is strongly peaked in the backward direction.

Using a lepton candidate with at least one hit in the microvertex detector, a \bar{D}^0 -lepton vertex was then fitted in space, and the lepton momentum vector was recomputed by imposing that its track originated at this new vertex. The precision of this secondary vertex was about $\pm 300 \mu\text{m}$ along the flight direction projected onto the plane transverse to the beam direction. The B^0 decay length was then defined as the signed distance between the primary vertex and the secondary \bar{D}^0 -lepton vertex. It was given the same sign as the scalar product of the \bar{D}^0 lepton momentum with the vector joining the primary to the secondary vertex. For the 1991-1993 data, the decay length was computed in the plane transverse to the beam axis and was required to be above 500 μm . For the 1994 data, with z information available from the VD, it was computed in space and was required to exceed 750 μm .

All other charged particles with momentum between 0.4 GeV/c and 4.5 GeV/c and charge opposite to that of the lepton were used as pion candidates for $D^{*-} \rightarrow \bar{D}^0\pi^-$ decay. This momentum range allowed the selection of D^{*-} with an energy fraction relative to the beam energy, $X_E(D^*) = E(D^*)/E_{\text{beam}}$, between 0.15 and 1. In order to reduce the combinatorial background, the impact parameter of this pion relative to the primary interaction vertex was required to be less than 3.0 mm. The momentum vector of the pion candidate was recomputed after imposing that its track originated at the \bar{D}^0 -lepton vertex. Then the selection of $D^{*-}\ell^+X$ events relied on the small mass difference (ΔM) between the D^{*-} and the candidate \bar{D}^0 .

As no kaon identification was required, some combinatorial background occurs in the $\bar{D}^0 \rightarrow K^+\pi^-\pi^+\pi^-$ decay mode when the K^+ and π^+ mass hypotheses are wrongly permuted. This is partly suppressed by applying a stronger mass difference constraint for this decay channel, the remaining combinations being described by an additional contribution to the background.

Figure 1a) shows the distribution of the mass difference $M(K^+\pi^-\pi^-) - M(K^+\pi^-)$ when the $K^+\pi^-$ invariant mass is within 70 MeV/c^2 of the nominal D^0 mass. Figure 1b) shows the invariant $K3\pi$ mass distribution when the mass difference value ΔM is within 2.1 (1.4) MeV/c^2 of the nominal ($D^{*-} - \bar{D}^0$) mass difference for 1991-1993 (1994) data. The different ΔM selections were applied in order to ac-

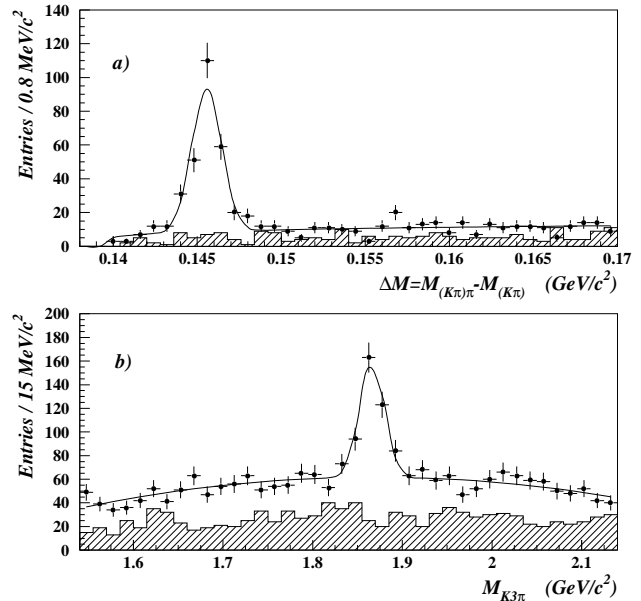


Fig. 1. The D^{*-} signals in the exclusive analysis: **a** $\Delta M = M(K^+\pi^-\pi^-) - M(K^+\pi^-)$ distribution and **b** $K^+\pi^-\pi^-\pi^+$ invariant mass distribution for events where the kaon candidate and the associated lepton in the same jet have the same charge (data points) or opposite charge (hatched histograms). The same selections are applied for the same and opposite charge events. A selection on $K\pi$ mass within 70 MeV/c^2 of the nominal D^0 mass is applied in **a**. A selection on the mass difference $M(K^+\pi^-\pi^-\pi^+\pi^-) - M(K^+\pi^-\pi^-\pi^+)$ was applied in **b** as explained in the text. The curves are the results of fits described in the text

count for the different resolutions in the two data samples. A clear signal corresponding to $D^{*-}\ell^+$ events is observed in each distribution when the kaon candidate and the lepton have the same charge (data points). The corresponding wrong sign $K^+\ell^-$ distribution (hatched histograms) is fitted with the same parameters as the $K^+\ell^+$ distribution in order to determine the contribution of $c\bar{c}$ events. A very small contribution is found which is subtracted later in this analysis. In Fig. 1a) the background is described by the function $\alpha(\Delta M - m_\pi)^\beta$ where α and β are free parameters. The $D^{*-} \rightarrow (K^+\pi^-)\pi^-$ signal is described by a Gaussian function with free normalization, mean value and width. The mean value (145.6 ± 0.1) MeV/c^2 obtained is compatible with the expected ($D^{*-} - \bar{D}^0$) mass difference and the resolution is $(0.9 \pm 0.1) \text{MeV}/c^2$.

The $K3\pi$ mass distribution of Fig. 1b) was fitted by using a second order polynomial for the combinatorial background, a Gaussian function for the $\bar{D}^0 \rightarrow K^+\pi^-\pi^-\pi^+$ events and a second Gaussian for events where the K^+ and π^+ masses were permuted. In the simulation, this second contribution amounted to 7% of the fitted signal, with a width 10% larger and a mean value 3 MeV/c^2 lower. The fitted mean value of the first Gaussian is $(1866 \pm 2) \text{MeV}/c^2$, in good agreement with the nominal D^0 mass [1], and the experimental resolution is $14 \pm 2 \text{MeV}/c^2$.

The total numbers of fitted $D^{*-}\ell^+$ events were 235 ± 19 in the $K\pi$ channel and 210 ± 25 in the $K3\pi$ channel.

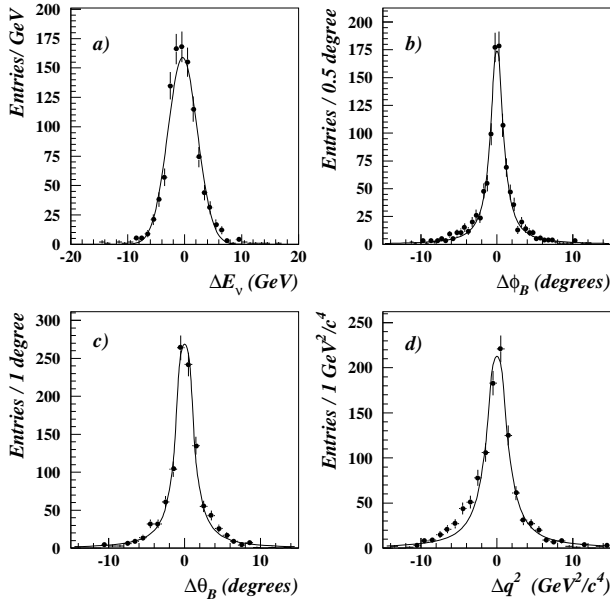


Fig. 2. Distributions of the difference between reconstructed variables and the true value in the simulation of the exclusive analysis of 1991-1993 data for **a** the neutrino energy E_ν , **b** the B meson azimuthal angle ϕ_B , **c** the B polar angle θ_B calculated with the energy-momentum constraint and **d** the reconstructed q^2 . The curves are Gaussian fits in **a** and Breit-Wigner ones in (**b-d**)

4.2 q^2 reconstruction

The four-momentum transfer squared in the $B^0 \rightarrow D^{*-}\ell^+\nu$ decay was reconstructed by measuring the B^0 meson four-momentum p_B and the D^{*-} meson four-momentum p_{D^*} . The experimental inputs used to determine the B hadron energy and momentum, in addition to the reconstructed D^{*-} and lepton, were the neutrino energy and the B hadron direction.

The neutrino energy E_ν was evaluated from the missing hemisphere energy E_{miss} corrected by a function of the $D^{*-}\ell^+$ energy, $F(E_{D^*\ell})$, determined from the simulation:

$$E_{miss} = \sqrt{s}/2 - E_{same} + \frac{m_{same}^2 - m_{oppo}^2}{2\sqrt{s}}$$

$$E_\nu = E_{miss} + F(E_{D^*\ell}),$$

where *same* and *oppo* refer to the hemispheres on the same and opposite sides relative to the $D^{*-}\ell^+$ system; m_{same} and m_{oppo} are the reconstructed invariant masses in each hemisphere and are included in order to correct the energy for events with more than two jets [18]. The function $F(E_{D^*\ell})$ was introduced to correct for losses due to experimental cuts and to detector inefficiencies. It was determined by parameterising the difference between the true neutrino energy and E_{miss} as a function of the $D^*\ell$ energy. If the neutrino energy obtained was negative, it was set to zero. Figs. 2a) and 3a) show the difference between the reconstructed and generated neutrino energy for $B^0 \rightarrow D^{*-}\ell^+\nu$ decays in simulated 1991-1993 and simulated 1994 data, respectively. A resolution of 2.7 GeV is reached in both cases, which corresponds to a relative error of $\pm 33\%$.

The B^0 meson direction was determined from its azimuthal angle ϕ_B in the plane transverse to the beam axis

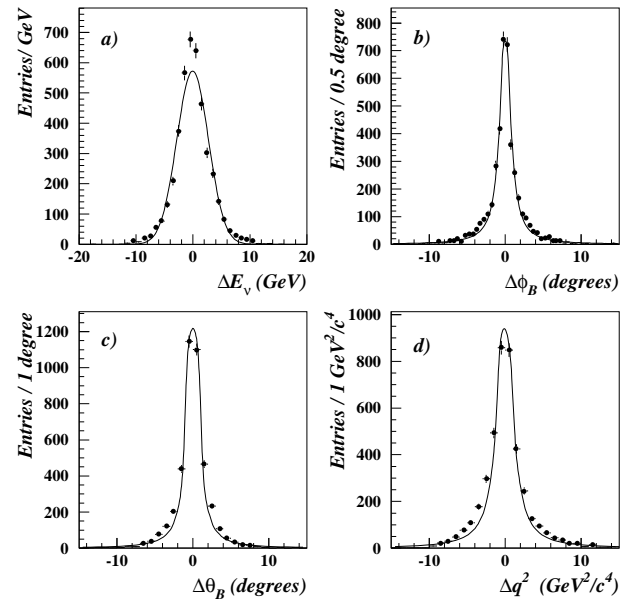


Fig. 3. Same as in Fig. 2, but for the simulation of 1994 data

and polar angle θ_B relative to the beam axis. For the 1994 data, where the microvertex detector provided a measurement of the z coordinate along the beam axis, both the azimuthal and polar angles were obtained from the oriented decay distance vector between the primary interaction vertex and the $D^{*-}\ell^+$ decay vertex. For the 1991-1993 data the neutrino energy and azimuthal angle (obtained as previously described) were used with the energy-momentum conservation constraint to determine θ_B . The quadratic ambiguity was resolved by taking the polar angle nearest to the thrust axis. Figs. 2b) and 3b) show the difference between the reconstructed and generated azimuthal angle in 1991-1993 and 1994 simulations, respectively. Resolutions of $\pm 1.4^\circ$ and $\pm 1.2^\circ$ were achieved in the two cases. Similar distributions are shown for θ_B on Figs. 2c) and 3c). The resolutions are $\pm 1.6^\circ$ and $\pm 1.2^\circ$ for 1991-1993 and 1994 simulations, respectively. Finally Figs. 2d) and 3d) show the difference between the estimated and generated q^2 values. Resolutions of $\pm 2.2 \text{ GeV}^2/c^4$ and $\pm 1.8 \text{ GeV}^2/c^4$ were achieved for the 1991-1993 and 1994 simulations.

The overall efficiency determined from a sample of fully simulated $B^0 \rightarrow D^{*-}\ell^+\nu$ decays was $(10.9 \pm 0.5)\%$ for $\bar{D}^0 \rightarrow K^+\pi^-$ and $(6.3 \pm 0.4)\%$ for $\bar{D}^0 \rightarrow K^+\pi^-\pi^+\pi^-$. Figure 4 shows the efficiency as a function of q^2 for each channel. A slight dependence is observed and an acceptance correction was applied.

5 Inclusive D^{*-} analysis

Only a limited fraction of D^0 decay final states were reconstructed with the exclusive technique described above. To increase the statistical precision of the measurement by exploiting a wider set of D^0 final states, an inclusive analysis was performed, inspired by the one originally proposed by the ARGUS collaboration at DESY [19]. The analysis was

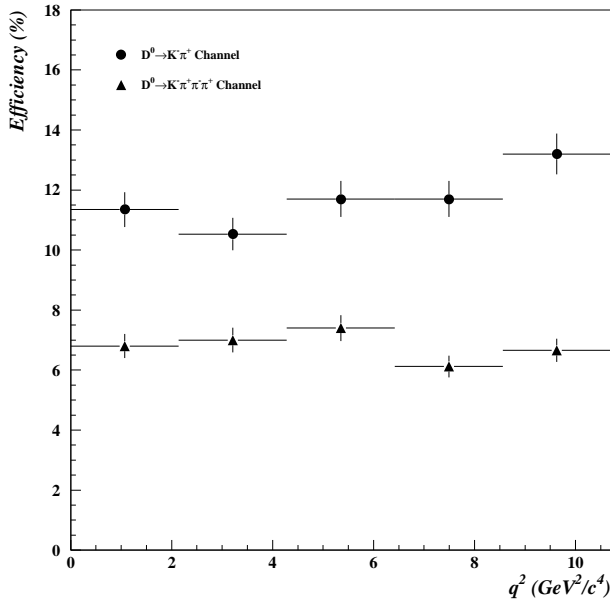


Fig. 4. Efficiency (%) as a function of the reconstructed q^2 in the exclusive analysis estimated from simulated $B^0 \rightarrow D^{*-} \ell^+ \nu$ events with $\bar{D}^0 \rightarrow K^+ \pi^- \pi^+ \pi^-$ (triangles) and $\bar{D}^0 \rightarrow K^+ \pi^-$ (points)

limited to the 1.37 million hadronic Z decays collected by DELPHI in 1994.

5.1 $D^{*-} \ell^+$ selection

The charged pion produced in the decay $D^{*-} \rightarrow D^0 \pi^-$ (hereafter referred to as the π^*) was used to tag D^{*-} particles. Due to the limited phase space available in the decay, the π^* is produced almost at rest in the D^{*-} rest frame. At LEP energies it receives a considerable Lorentz boost (when the D^{*-} is produced from B hadron decays, the average π^* energy is about 1.5 GeV), but it can be tagged by the low momentum carried in the plane orthogonal to the boost direction. The method has previously been applied by the DELPHI collaboration to extract the partial width of the decay of the Z to $c\bar{c}$ final states [20]. In the following a refinement of this technique is described which improves the rejection of the background.

The sample of hadronic Z decays was enriched in $b\bar{b}$ events by applying the b-tagging algorithm already used by the DELPHI collaboration for several analyses [21]. Jets in which a lepton is present were then selected. Tighter lepton selection criteria were applied than for the exclusive analysis. The lepton transverse momentum was then required to be $p_T^\ell > 1$ GeV/c.

Any particle with charge opposite to that of the lepton was considered as a candidate for D^{*-} tagging if its squared momentum p_T^2 transverse to the jet direction was below 0.03 GeV²/c⁴. In the simulation, this cut removes only 2 % of the pions from D^{*-} decays. Furthermore, the momentum of the selected particle had to be in the range $0.5 < p < 2.5$ GeV/c. If more than one candidate was selected inside a jet, all possible combinations were considered

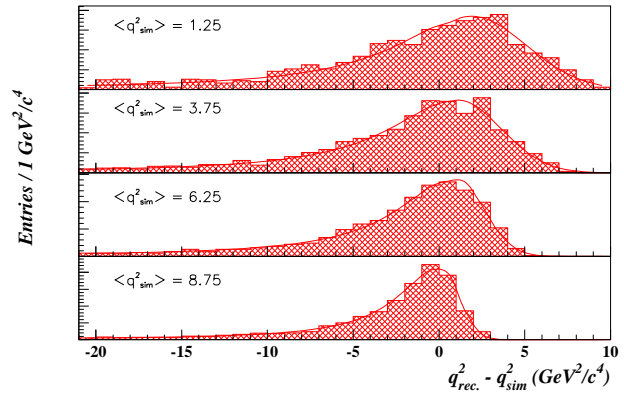


Fig. 5. Difference between the reconstructed and simulated q^2 for the inclusive analysis, for increasing values of the simulated q^2 . The curves show the parameterisations described in the text

in turn. Particles with the same charge as the lepton but otherwise surviving the above selection were used to check the description of the background in the simulation.

An inclusive reconstruction of D^0 decays was then performed by considering all the particles in the jet, apart from the lepton and the selected pion. A considerable fraction of the particles are produced in the primary fragmentation process. These were removed by exploiting the long lifetime and the large Lorentz boost of B^0 mesons. The method is a refinement of the technique already applied by DELPHI in ref. [22]. The probability that a track from a charged particle originated from the primary interaction vertex was evaluated on the basis of its impact parameter and its error [21]. Charged particles with either low probability or high rapidity relative to the jet direction were then selected. Neutral particles with rapidity above 1.5 were also used. The D^0 four-momentum was then evaluated as the sum over all selected particles. In the simulation the average mass of the reconstructed state is consistent with the D^0 mass and the spread of the mass distribution is about 700 MeV/c² due to inefficiencies and residual contaminations. Events were further selected by requiring the D^0 reconstructed mass to be between 0.5 GeV/c² and 3 GeV/c². Events for which the D^0 energy exceeded 25 GeV were rejected. The D^{*-} was then built by adding the four-momentum of the tagging pion to that of the D^0 . According to the simulation, this procedure reproduced the true D^{*-} direction with a precision of $\sim 2.4^\circ$, to be compared with $\sim 3.5^\circ$ obtained when using instead the jet direction as an estimate. Events containing a D^{*-} were finally selected by looking at the mass difference ΔM between the D^{*-} and the reconstructed D^0 .

5.2 Event kinematics and q^2 reconstruction

Due to the limited phase space available, a strong correlation holds between the momentum of the D^{*-} and that of the π^* . The most precise unbiased estimator of the D^{*-} energy was then obtained by properly parameterising it as a function of the momentum of the π^* . This gave the D^{*-} energy with $\sim 14\%$ relative precision.

The energy of the neutrino was estimated from the missing energy, as in the exclusive D^{*-} reconstruction. In the

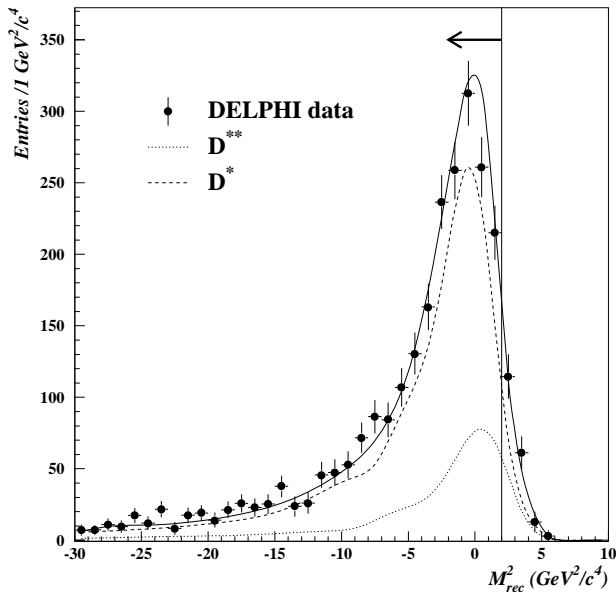


Fig. 6. Squared missing mass (M_{rec}^2) recoiling against the $D^{*-} \ell$ system for the inclusive analysis. The dots represent the data, after subtraction of the combinatorial background and other background sources different from D^{**} . The continuous line shows the signal expected from the simulation (D^{*-} and D^{**}), the dashed line is the contribution from semileptonic decays of B mesons to D^{*-} , the dotted line is the contribution from semileptonic decays of B mesons to D^{**} . The arrow indicates the cut $M_{\text{rec}}^2 < 2 \text{ GeV}^2/c^4$ which was applied to reduce the amount of D^{**} in the sample used for the analysis

inclusive analysis the resolution on the neutrino energy was found to be about 4 GeV.

The B^0 decay vertex was not reconstructed. Its flight direction was estimated by exploiting momentum conservation. The three-momenta of all particles in the event, except the lepton and the tracks assigned to the D^{*-} , were added. The resulting direction was then reversed and considered to be the B^0 direction. The resolution obtained with this algorithm was $\sim 1.5^\circ$ in both the azimuthal and the polar angles.

Simulated events were used to study the q^2 resolution. The simulation shows a linear dependence of the mean reconstructed q^2 on the generated one. The resolution however depends on the actual value of q^2 , improving at higher values, as seen in Fig. 5. The simulation shows that the tails towards low values of the reconstructed q^2 are mostly due to events where the direction of the B^0 was poorly determined. The resolution was parameterised by a Breit-Wigner function if the difference between the reconstructed and the generated value of q^2 was smaller than a discriminant value, otherwise a Gaussian function was used. The dependence of the widths and of the point of connection of the two functions on the true q^2 was determined from the simulation.

A set of tests was performed to check that the simulation described the data with the accuracy needed. Excellent agreement was always found. Figure 6 shows for instance the reconstructed missing mass squared (M_{rec}^2) of the system recoiling against the $D^{*-} \ell^+$ (representing the neutrino mass in the decay $B^0 \rightarrow D^{*-} \ell^+ \nu$) compared to the simulation expectation, after subtracting the combinatorial background

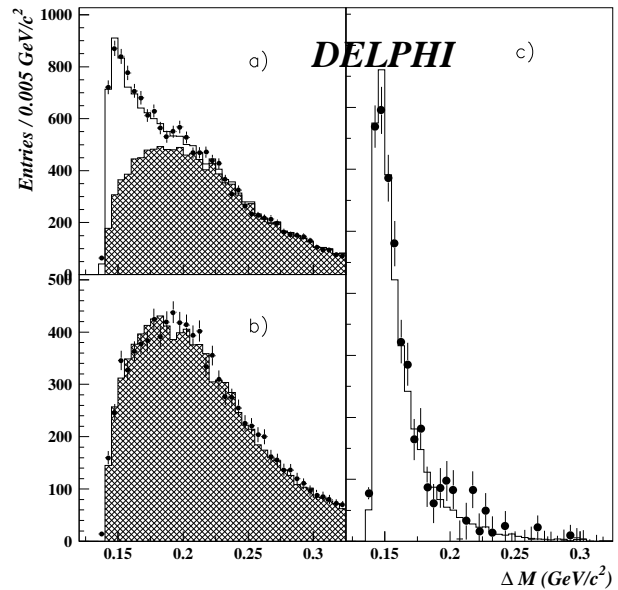


Fig. 7. $\Delta M = M_{D^{*-}} - M_{D^0}$ distribution for the inclusive analysis, when the lepton and the π^* have **a** opposite charge and **b** same charge. The dots are the data, the shadowed area shows the prediction of the simulation for the combinatorial background. The experimental distribution, after subtraction of the simulated background, is compared to the sum of all expected D^{*-} sources in **c**

taken from the simulation. Both the central width and the tails are well reproduced. The simulation shows that events produced from background processes tend to accumulate at higher M_{rec}^2 values. In the case of D^{**} production (see next section) this is due to the production of additional pions not considered in the reconstruction of the state. To reduce this source of background contamination, M_{rec}^2 was required to be below $2 \text{ GeV}^2/c^4$.

Figure 7 shows the ΔM distributions for the selected events in which the lepton and the π^* have opposite or same charges. The hatched area shows the shape of the combinatorial background in the simulation. The samples were normalised using events in the side band region defined by $0.2 < \Delta M < 0.4 \text{ GeV}/c^2$. Figure 7c) compares the data (after subtracting the combinatorial background estimated from the simulation) with simulated events containing a $D^{*-} \ell^+$ final state. Only events satisfying the above selection and also having $\Delta M < 0.17 \text{ GeV}/c^2$ were considered as D^{*-} candidates. After subtracting the combinatorial background, 2420 ± 69 (-36 ± 44) candidate D^{*-} -lepton events were found in the opposite (same) charge sample. The quoted errors are statistical only.

The overall efficiency to reconstruct a genuine $B^0 \rightarrow D^{*-} \ell^+ \nu$ event was $(11.3 \pm 0.5) \%$, where the error contains the systematic uncertainties. Figure 8 shows the dependence of the efficiency on q^2 and, superimposed, the linear parameterisation adopted to describe the effect.

6 Evaluation of D^{**} fraction

An important source of background is due to the process $B \rightarrow D^{*} \ell \nu X$ which includes resonant $B \rightarrow D_j^{(*)} \ell \nu$ decays (fol-

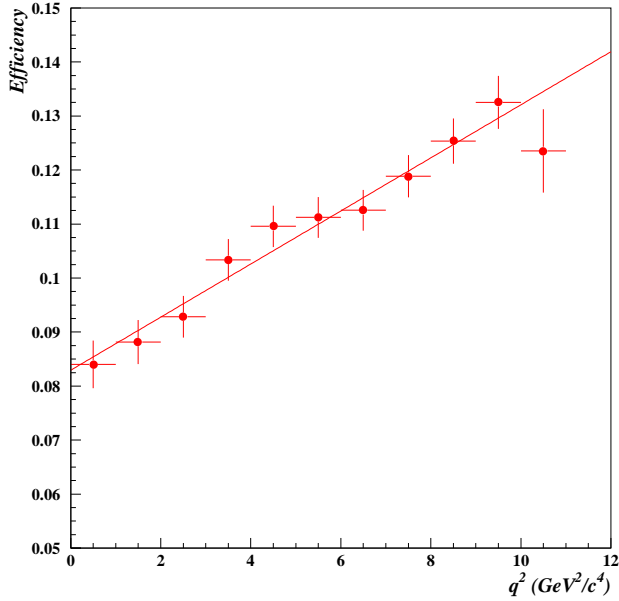


Fig. 8. Variation of the efficiency as a function of the generated q^2

lowed by $D_J^{(*)} \rightarrow D^* \pi$ as well as non-resonant decays. All these states are often referred to as D^{**} . Their amount in the data sample was directly measured by looking for a charged pion coming from the $D^* \ell$ vertex. Isospin conservation was then used to estimate the value of

$$R = \frac{Br(B \rightarrow D^{*-} \ell^+ \nu X)}{Br(B \rightarrow D^{*-} \ell^+ \nu X) + Br(B^0 \rightarrow D^{*-} \ell^+ \nu)},$$

where X represents neutral or charged particles.

The measurement used the exclusively reconstructed D^* sample. The analysis was restricted to events from the decay channel $D^{*-} \rightarrow (K^+ \pi^-) \pi^-$ to reduce the combinatorial background. To take advantage of the new microvertex detector, only the 1994 data set was used.

To increase the sample size, the cut on the lepton transverse momentum p_T^ℓ was loosened to $0.2 \text{ GeV}/c$. The mass difference $M(D^0 \pi) - M(D^0)$ was required to be within $2 \text{ MeV}/c^2$ of the nominal mass difference and the mass of the reconstructed D^0 was required to be within $50 \text{ MeV}/c^2$ of the nominal value. Furthermore, the selection criteria were optimized to improve the secondary vertex resolution. The decay length was required to be greater than 0.75 mm , the χ^2 probability of the D^0 vertex fit had to be higher than 1%, and the χ^2 of the $D^* \ell$ vertex fit had to be less than 20. Tracks were considered only if the error on their impact parameter to the primary vertex was below 0.5 mm . Furthermore the error on the impact parameter computed to the $D^* \ell$ vertex had to be less than 1.5 mm .

Particles other than those forming the D^* and lying in the same hemisphere were used provided their charges were the same as that of the lepton. The significance S_2 was defined as the impact parameter, reconstructed in space with respect to the $D^* \ell$ vertex, divided by its error.

The track with the lowest S_2 was chosen as a candidate pion from the $B \rightarrow D^{*-} \pi^+ \ell^+ \nu(X)$ decay. In $B^0 \rightarrow D^{*-} \ell^+ \nu$

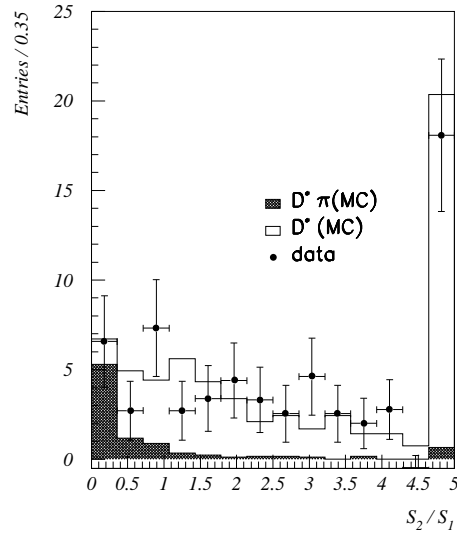


Fig. 9. S_2/S_1 distributions for background subtracted data (dots) and simulation. Hatched area is the contribution of $D^* \pi$ events in the simulation. The last bin contains the events in overflow

events, the selected pion candidate is a fragmentation particle originating from the primary vertex. To discriminate better between these events and $B \rightarrow D^{*-} \pi^+ \ell^+ \nu(X)$ events, the significance S_1 of the impact parameter of the selected pion with respect to the primary vertex was also considered. S_1 should be larger for $B \rightarrow D^{*-} \pi^+ \ell^+ \nu(X)$ events and smaller for $B^0 \rightarrow D^{*-} \ell^+ \nu$ events while S_2 should behave in the opposite way. The best separation between the two event classes was obtained using the ratio S_2/S_1 .

Figure 9 shows the distribution of S_2/S_1 for the background subtracted data and for the dedicated Monte Carlo simulation of $B \rightarrow D^{*-} \pi^+ \ell^+ \nu(X)$ and $B^0 \rightarrow D^{*-} \ell^+ \nu$ events. The region near zero is populated mostly by $D^* \pi$ events while the rest of the distribution is dominated by D^* events.

The background was estimated to be 20% using events lying in the signal band of the ΔM distribution but with the wrong D^* lepton charge correlation. The shape of the S_2/S_1 distribution for the background was studied using events lying in the sidebands of the ΔM distribution with either a) the correct or b) the wrong charge correlation and c) events in the ΔM signal band but with wrong charge correlation. The normalized background was subtracted and the difference in the results from the three samples defined above used to determine the contribution to the systematic error.

To extract the numbers of D^* and $D^* \pi$ events the experimental distribution was divided into two parts at $S_2/S_1 = 0.6$. The expected fractions of D^* and $D^* \pi$ events in the two bins were evaluated with the simulation. It was found that 5% of the D^* events and 77% of the $D^* \pi$ events have $S_2/S_1 < 0.6$. The fraction R was computed:

$$R = \frac{k N_{D^* \pi}}{k N_{D^* \pi} + \frac{\epsilon_{D^* \pi}}{\epsilon_{D^*}} N_{D^*}},$$

where $\frac{\epsilon_{D^* \pi}}{\epsilon_{D^*}}$ is the efficiency ratio between the $D^* \pi$ and D^* events, determined in the simulation to be 1.33 ± 0.02 , and k takes into account the decay $B^0 \rightarrow D^{*-} \pi^0 \ell^+ \nu$. This factor was estimated assuming that B^+ and B^0 particles have equal

semileptonic partial widths and lifetimes [23], that $D^{*}\pi$ states are produced with a fixed isospin ($I=1/2$) and that isospin is conserved:

$$k = \frac{Br(B^+ \rightarrow D^{*-}\ell^+\nu\pi^+) + Br(B^0 \rightarrow D^{*-}\ell^+\nu\pi^0)}{Br(B^+ \rightarrow D^{*-}\ell^+\nu\pi^+)} = 1.5.$$

Including other possible final states with $D^*\pi\pi$ and the channel $B_s^0 \rightarrow D^{*-}\ell^+\nu K^0$ with $K^0 \rightarrow \pi^+\pi^-$ and making some assumptions about the decay rates and efficiencies gives $k = 1.45$. The difference between the two values was included in the systematic error.

Another source of systematic error was estimated by varying the S_2/S_1 cut from 0.2 to 1.0. The full systematic error is a sum in quadrature of all three contributions and the final value of R obtained was:

$$R = 0.19 \pm 0.10(\text{stat}) \pm 0.06(\text{syst}).$$

7 Other backgrounds

Other sources of background were estimated using the simulation.

The $B^0 \rightarrow D^{*-}\tau^+\nu$ decay (with the τ decaying leptonically) and $B \rightarrow D^{*}\bar{D}$ (with the \bar{D} meson decaying semileptonically) also give $D^{*-}\ell^+$ candidates. These were suppressed by the lepton p_T^ℓ requirement.

The decay $B^0 \rightarrow D^{*}(n)\pi$ should also present some excess of right sign $D^{*}\pi^+$ candidates when a pion is wrongly identified as a lepton.

True D^{*-} with a fake lepton ℓ^+ in the same jet can be present in $c\bar{c}$ events if a pion is wrongly identified as a lepton. This background was strongly reduced by the p_T^ℓ and decay length selections. It was considered to be negligible in the inclusive analysis, where no D^{*-} signal was observed in the mass distribution of wrongly charge correlated events (see Fig. 7b), and it was directly subtracted in each q^2 bin for the exclusive analysis. This subtraction also corrects for the small background in the $K3\pi$ channel of real \bar{D}^0 mesons associated with a random π^- .

The branching fractions and the errors assumed for the processes involved in the analysis are listed in Table 1. A relative error of $\pm 50\%$ was assumed for the process $B^0 \rightarrow D^{*}(n)\pi$, accounting for the uncertainties both on the production rate and on the lepton faking probability. The content of the fitted $D^{*-}\ell^+$ sample is detailed in Table 2.²

8 Determination of $|V_{cb}|$ and of branching fractions

The branching fraction $Br(B^0 \rightarrow D^{*-}\ell^+\nu)$ was obtained from the number, $N_{D^*\ell}$, of $D^*\ell$ candidates which were left after background subtraction:

$$Br(B^0 \rightarrow D^{*-}\ell^+\nu) = \frac{N_{D^*\ell}}{\epsilon_{D^*\ell} N_{B^0}},$$

where $\epsilon_{D^*\ell}$ is the reconstruction efficiency including detector acceptance for this decay channel and N_{B^0} is the number

² The $B_s^0 \rightarrow D^{*}\bar{K}^0\ell^+\nu_\ell$ contribution is included in the second line of the table

Table 1. Summary of the relevant inputs used in the analysis

	Input parameters	Ref.
R_b	22.19 ± 0.17 (%)	[24]
$Br(b \rightarrow \bar{B}^0)$	38.5 ± 2.1 (%)	[25]
τ_{B^0}	1.57 ± 0.05 ps	[23]
$Br(B^0 \rightarrow D^{*}\tau^+\nu)$	2.1 ± 0.4 (%)	[10]
$Br(B \rightarrow D^{*}X_c, X_c \rightarrow \ell^+\nu Y)$	0.33 ± 0.15 (%)	[1]
$Br(B^0 \rightarrow D^{*}(n)\pi)$	6.1 ± 3.1 (%)	[1]
$Br(D^{*+} \rightarrow D^0\pi^+)$	68.1 ± 1.3 (%)	[1]
$Br(D^0 \rightarrow K^-\pi^+)$	4.01 ± 0.14 (%)	[1]
$Br(D^0 \rightarrow K^-\pi^+\pi^-\pi^+)/Br(D^0 \rightarrow K^-\pi^+)$	2.02 ± 0.11	[1]

Table 2. Composition (%) of the $D^{*-}\ell^+$ data sample

	Exclusive	Inclusive
$B^0 \rightarrow D^{*-}\ell^+\nu$ signal	76.3	84.6
$B \rightarrow D^{*}\ell^+\nu X$	13.2	11.3
$B^0 \rightarrow D^{*}\tau^+\nu$	2.7	1.6
$B \rightarrow D^{*}\bar{D}$	2.9	0.8
$B^0 \rightarrow D^{*}(n)\pi$	4.8	1.7
Total	100	100

of B^0 hadrons produced. The number of B^0 hadrons was computed from the number, N_Z , of Z hadronic decays, the Z partial width into $b\bar{b}$ quarks divided by the Z partial width into $q\bar{q}$ ($R_b = \frac{\Gamma_{b\bar{b}}}{\Gamma_{had}}$), and the probability of a b quark fragmenting to a B^0 :

$$N_{B^0} = 4N_Z R_b Br(b \rightarrow \bar{B}^0). \quad (1)$$

The factor 4 accounts for the fact that B^0 mesons can be produced in either hemisphere and ℓ can be either e or μ . The probability of a b quark fragmenting to a B^0 was extracted as in ref. [25], by comparing the average B meson mixing probability at LEP with that obtained for B^0 mesons at $\mathcal{T}(4S)$ and from time dependent oscillation measurements. Maximal mixing was assumed for B_s mesons and the fraction of b quarks fragmenting to b -baryons was taken to be $(13 \pm 4)\%$.

The result for $|V_{cb}|$ was obtained by fitting the measured q^2 distribution according to the HQET prediction for the differential decay width, expressed in terms of the scalar product y of the four-velocities of the B and D mesons:

$$y = v_B \cdot v_{D^*} = \frac{m_B^2 + m_{D^*}^2 - q^2}{2m_B m_{D^*}}.$$

Then

$$\begin{aligned} \frac{d\Gamma}{dy} &= \frac{1}{\tau_{B^0}} \frac{dBr(B^0 \rightarrow D^{*-}\ell^+\nu)}{dy} \\ &= \frac{G_F^2}{48\pi^3 \hbar} m_{D^*}^3 (m_B - m_{D^*})^2 F^2(y) |V_{cb}|^2 \sqrt{y^2 - 1} \\ &\quad \times \left[4y(y+1) \frac{1-2yr+r^2}{(1-r)^2} + (y+1)^2 \right]. \end{aligned} \quad (2)$$

where $r = m_{D^*}/m_B$. For the unknown form factor $F(q^2)$ a linear development was used:

$$F(q^2) = F(q_{max}^2) \left(1 + a^2 \frac{q_{max}^2 - q^2}{2m_B m_{D^*}} \right).$$

In both analyses the two parameters $F(q_{max}^2)|V_{cb}|$ and a^2 were left free in the fit.

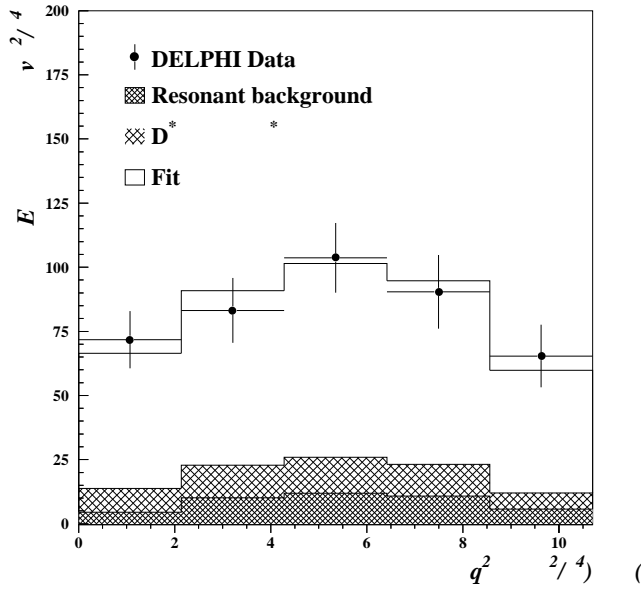


Fig. 10. The q^2 spectrum in the exclusive analysis (dots) compared to the results of the fit (line). The white area shows the fitted contribution from signal events, the hatched areas show the background composition. The fits to the ΔM or M distributions allow the number of signal events to be extracted in each q^2 bin. Therefore the combinatorial background is not displayed

8.1 Exclusive analysis

The allowed kinematical range in q^2 from 0 to $10.7 \text{ GeV}^2/c^4$ was divided into five equal bins of $2.14 \text{ GeV}^2/c^4$, comparable to the q^2 resolution of $2.0 \text{ GeV}^2/c^4$. The number of signal events in each bin was determined by a fit to the distribution of the mass difference $\Delta M = M(K\pi\pi) - M(K\pi)$ for $\bar{D}^0 \rightarrow K^+\pi^-\pi^-\pi^+$ decays, as described in section 4.1. For $\bar{D}^0 \rightarrow K^+\pi^-\pi^+\pi^-\pi^+$ decays, the number of signal events was obtained from a fit to the $(K3\pi)$ mass distribution.

The backgrounds listed in Table 2 were treated as follows. Due to the p_T^ℓ selection, the reconstruction efficiency is lower for a B meson decaying into a D^{**} than for a direct decay into a D^* meson. For $p_T^\ell > 0.8 \text{ GeV}/c$, the reduction factor is 0.74 ± 0.12 in the simulation. The reconstructed q^2 distribution of simulated $B \rightarrow \bar{D}^{**}\ell^+\nu$ events was normalized to the result of section 6 and then subtracted. The q^2 distribution of other resonant background sources was estimated according to the simulation and normalized as in Table 2. The overall q^2 distribution is presented in Fig. 10.

From the background subtracted sample, the following branching fraction is measured:

$$Br(B^0 \rightarrow D^{*-}\ell^+\nu) = (4.91 \pm 0.45)\%,$$

where the error is statistical only.

A binned χ^2 fit was performed on the background subtracted q^2 spectrum to the function given in (2) convoluted with the experimental resolution functions shown in Figs. 2d) and 3d). The result is:

$$F(q_{max}^2)|V_{cb}| = (34.2 \pm 3.4) \cdot 10^{-3}$$

$$a^2 = 0.77 \pm 0.26,$$

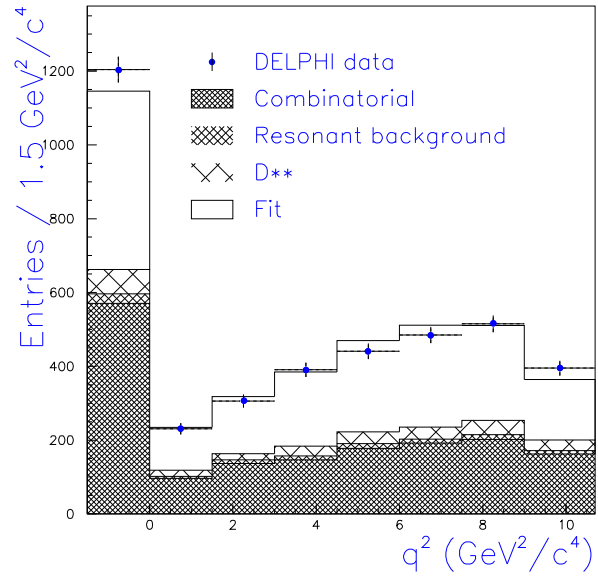


Fig. 11. The q^2 spectrum in the inclusive analysis (dots) compared to the result of the fit (line). All events outside the physical range have been grouped in a single bin. The white area shows the fitted contribution from signal events, the hatched areas show the background composition

where the errors are statistical only. The correlation coefficient between the two fitted parameters is 90.6 % and the χ^2 of the fit is 1.80 for 3 degrees of freedom.

8.2 Inclusive analysis

The results of section 6 were used to determine the composition of the sample. Of the 2420 selected candidates after combinatorial background subtraction, 99 were attributed to background sources other than D^{**} production. The $p_T^\ell > 1 \text{ GeV}/c$ and the $M_{rec}^2 < 2 \text{ GeV}^2/c^4$ cuts reduce the efficiency to tag a B decay to a D^{**} state by a factor 0.57 with respect to one to a D^{*-} state. Taking all efficiency corrections into account, the following branching fraction is obtained:

$$Br(B^0 \rightarrow D^{*-}\ell^+\nu) = (5.65 \pm 0.17)\%,$$

where the error is statistical only.

To determine $|V_{cb}|$, events were grouped in bins of q^2 , each $1.5 \text{ GeV}^2/c^4$ wide. The fraction of events from background sources in each bin was determined from the simulation tuned as described above. Only events with q^2 greater than $-50 \text{ (GeV}^2/c^4)$ were used. This removed 5.0 % (3.5%) of the signal in the data (simulation). A χ^2 fit was then performed comparing the number of events observed in each bin to the number expected, which was obtained by adding the predicted background to the convolution of the model function (see (2)) and the experimental resolution function (see section 5.2), integrated inside the bin. The result was:

$$F(q_{max}^2)|V_{cb}| = (35.9 \pm 2.2) \cdot 10^{-3}$$

$$a^2 = 0.74 \pm 0.20,$$

where the errors are statistical only. It should be noted that the branching ratio for the considered decay can be obtained

from the fitted values of a^2 and $|V_{cb}|$ by integrating (2). The value so obtained is 5.37 %. The discrepancy with the result obtained above is due to the uncertainties in the parametrisation of the resolution function and in the variation of the efficiency with q^2 . The effect of such uncertainties on the systematic error is discussed in section 9.2 below. The comparison between the fitted result and the experimental data is shown in Fig. 11. The probability of the fit is 8 %. If only events with q^2 greater than $-10 \text{ GeV}^2/c^4$ were used, the fit probability would increase to 24 % while $|V_{cb}|$ would vary by 0.7×10^{-3} .

9 Systematic uncertainties

The different sources of systematic uncertainties considered are reported in Table 3. Several are common to the two analyses, namely the overall normalisation, the efficiency determination and the background subtraction.

The overall normalisation depends on the knowledge of R_b , on the probability that a b quark fragments to a B^0 meson, and on the B^0 lifetime τ_{B^0} (see (1) and (2)). All these quantities were varied inside the bounds allowed by present measurements (see Table 1), and the corresponding variations of the measured quantities were added to the systematic error. The errors due to the uncertainties on the D^{*-} and D^0 decay branching fraction were computed in the same way.

About 10 % of the tracks from low momentum charged particles are lost due to cracks or interactions with the detector material before the TPC. The error on the tracking efficiency was estimated from studies of the material [26] and of the TPC cracks. This uncertainty affects the exclusive and inclusive analyses in a different way. Conservatively 6% (3%) systematic error was assigned to the exclusive (inclusive) analysis.

Lepton identification was studied on a sample of events with high lepton purity, namely electrons from photon conversion and from radiative Bhabha events, and muons from τ decays and from $\gamma\gamma \rightarrow \mu^+\mu^-$. Compared to the prediction from the simulation, relative inefficiencies of 0.965 ± 0.03 , 0.945 ± 0.017 and 1.005 ± 0.02 were found for electrons, loose muons and standard muons, respectively.

The reconstruction efficiency depends on the B^0 energy due to the vertex and momentum cuts. The systematic error due to the uncertainty on the average fraction, $\langle x_E \rangle$, of the beam energy carried by B hadrons from Z decays was evaluated assuming the $\langle x_E \rangle$ value measured by DELPHI, $\langle x_E \rangle = 0.702 \pm 0.009$ [28].

The efficiency of the kinematical cuts was computed in the simulation. In principle this introduces a model dependence. The effect has already been studied by the CLEO collaboration, which adopted more severe cuts. They compared events simulated with four different decay models [9] and observed a spread of 1.2% for the values of the efficiency. In the present analysis the systematic error was computed by iteration. The simulated spectrum was corrected to the experimental values and the dependence of the efficiency on q^2 computed again. Then the analysis was repeated with the new efficiency correction. After the first iteration the values

changed by $\sim 1\%$. This was taken as the systematic error and no further iteration was performed.

The following subsections discuss the systematic errors peculiar to the exclusive and inclusive analyses respectively.

9.1 Exclusive analysis

In the exclusive analysis the following further sources of uncertainty were considered.

The uncertainty on the D^* selection was computed by varying the cuts and summing all the resulting variations in the branching ratio and in $|V_{cb}|$. Table 4 summarizes the following contributions:

- The effect of the B^0 flight distance cut was checked by removing it. The measured branching ratio changed by 0.7% and 0.3% for the $\bar{D}^0 \rightarrow K^+\pi^-$ and $\bar{D}^0 \rightarrow K^+\pi^-\pi^+\pi^-$ channels, respectively.
- The requirement on the impact parameter of tracks with respect to the D^0 vertex in the $\bar{D}^0 \rightarrow K^+\pi^-\pi^+\pi^-$ channel was also varied from 100 to 400 μm and the branching ratio recomputed in each case. A difference of $\pm 1.9\%$ was found.
- To take into account the different resolutions, the mass cuts applied in the simulation were adjusted in order to provide the same relative efficiency as in the data. The cuts were varied inside the statistical error of the fitted width of the signal and errors of $\pm 3.4\%$ and $\pm 3.7\%$ were found for the $\bar{D}^0 \rightarrow K^+\pi^-$ and $\bar{D}^0 \rightarrow K^+\pi^-\pi^+\pi^-$ channels.
- The effect of the selection on the impact parameter of the pion from D^{*-} decay was checked: 5% more events were selected in the simulation than in the data. A 5% correction was applied on the efficiency and an error of $\pm 3\%$ was estimated.
- The statistical error on the overall efficiency due to the finite size of the simulation sample was finally added.

The resulting systematic uncertainty on the D^* selection was $\pm 4.4\%$.

In addition, the effect of the B^0 lifetime was studied by varying the distance cut in the same way as the lifetime. A $\pm 0.7\%$ error on the branching ratio was inferred and was added to the B^0 lifetime systematic computed previously (see first line of Table 3).

The results of sections 6 and 7 were used to determine the uncertainty on the total amount of physics background. The effect of the uncertainty on the D^{**} amount was estimated by varying the measured value inside the error. The corresponding systematic error was $\pm 10.6\%$ on the branching ratio and $\pm 5.3\%$ on $|V_{cb}|$.

The effect of the uncertainty on the other sources of physics background was obtained by varying in the simulation their branching fractions inside the measurement errors (see sections 6 and 7). Furthermore the results were computed assuming a flat q^2 distribution for the physics background. The total variation was $\pm 2.4\%$ on the branching ratio and $\pm 1.9\%$ on $|V_{cb}|$.

For the $|V_{cb}|$ measurement only reconstructed events with q^2 inside the physical limits were used: $(94.0 \pm 2.5)\%$

Table 3. Systematic uncertainties on $Br(\mathbf{B}^0 \rightarrow \mathbf{D}^{*-} \ell^+ \nu)$, $|V_{cb}|$ and a^2 for the inclusive and exclusive analyses. Uncorrelated errors are flagged by (u)

	$\Delta Br/Br$ (\mathbf{D}^*) %		$\Delta V_{cb} / V_{cb} $ %		Δa^2	
	incl.	excl.	incl.	excl.	incl.	excl.
$\tau(\mathbf{B}^0)$	—	± 0.7	± 1.6	± 2.0	—	± 0.01
R_b	± 0.8	± 0.8	± 0.4	± 0.4	—	—
$Br(\mathbf{b} \rightarrow \mathbf{B}^0)$	± 5.5	± 5.5	± 2.7	± 2.7	—	—
$Br(\mathbf{D}^{*-} \rightarrow \mathbf{D}^0 \pi^-)$	± 2.0	± 2.1	± 1.0	± 1.0	—	—
$Br(\mathbf{D}^0 \rightarrow \mathbf{K}(3)\pi)$ (u)	—	± 5.6	—	± 2.8	—	—
Tracking efficiency	± 3.0	± 6.0	± 1.5	± 3.0	—	—
Lepton identification	± 2.0	± 2.0	± 1.0	± 1.0	—	—
$\langle x_E \rangle$	± 1.8	± 1.2	± 0.9	± 0.6	—	—
Model dependence	± 1.0	± 1.0	± 1.0	± 1.0	—	—
b-tagging (u)	± 3.7	—	± 1.9	—	—	—
\mathbf{D}^{*-} selection (u)	± 2.5	± 4.4	± 1.3	± 2.2	—	—
Combinatorial background (u)	$^{+2.0}_{-5.4}$	—	± 1.1	—	$+0.06$	—
\mathbf{D}^{**} fraction	± 8.2	± 10.6	± 4.1	± 5.3	—	± 0.03
Other B decays and fake leptons	± 1.4	± 2.4	± 0.8	± 1.9	—	± 0.04
Fit systematic and resolution (u)	—	—	± 3.2	± 1.5	$^{+0.17}_{-0.16}$	± 0.09
Total	$^{+12.1}_{-13.1}$	± 15.7	± 7.1	± 8.4	$^{+0.18}_{-0.16}$	± 0.10

Table 4. Relative systematic uncertainties (%) on the efficiencies for the two channels considered in the exclusive analysis

Channel	Distance	Impact par.	Mass	π^*	M-C stat.	Total
$\overline{\mathbf{D}}^0 \rightarrow \mathbf{K}^+ \pi^-$	0.7	—	3.4	3.	1.7	4.9
$\overline{\mathbf{D}}^0 \rightarrow \mathbf{K}^+ \pi^- \pi^+ \pi^-$	0.3	1.9	3.7	3.	2.6	5.8
Total	0.4	0.9	2.5	3.	1.6	4.4

of events were selected in the data, in good agreement with the $(93.1 \pm 0.3)\%$ found in the simulation. No uncertainty was taken into account for this selection.

The parameters of the resolution function used in the fit were varied by a factor 2. The resulting $\pm 1.5\%$ and $\pm 15\%$ variations observed on $|V_{cb}|$ and a^2 were considered as systematic errors.

9.2 Inclusive analysis

The efficiency of the b-tagging algorithm employed in the inclusive analysis was measured using a high p_T^ℓ lepton sample with a method similar to that described in [24]. The fractions of b-tagged events were compared with the fraction of events with a high p_T^ℓ lepton in data and simulation. A correction factor of 0.938 ± 0.035 to the efficiency predicted by the simulation was found. The error on this factor was translated into a corresponding uncertainty on the b-tagging efficiency ($\pm 3.7\%$) and hence on the branching ratio.

The efficiency of the \mathbf{D}^* reconstruction was checked by varying the cuts. Removing the cuts on the \mathbf{D}^0 mass and energy changed the measured branching ratio by 0.2%. The ΔM requirement was varied between 0.15 and 0.20: the resulting variation was 2%. The \mathbf{D}^0 mass and energy in the simulation were shifted by 0.1 GeV/c^2 and 0.5 GeV/c^2 respectively to match the data. The analysis was repeated without that tuning and the variation was 1.5%. The M_{rec}^2 cut was either removed or tightened (to $M_{\text{rec}}^2 < 0.5 \text{ GeV}^2/c^4$): the effect was negligible and no systematic error was considered. The \mathbf{D}^0 reconstruction efficiency in this analysis

could in principle be different for different final states from the \mathbf{D}^0 decay, as different criteria to select charged and neutral particles were employed. The efficiency was therefore computed in the simulation as a function of the fraction of charged particles selected. No dependence was observed and no systematic error was assigned. The average fractions of charged particles were 0.584 ± 0.001 and 0.580 ± 0.003 in the simulation and in the data respectively. A total systematic error of $\pm 2.5\%$ on the efficiency of the \mathbf{D}^* reconstruction was obtained by summing the three contributions found.

The effect of the combinatorial background was evaluated in the data using side bands and events with wrong charge correlation. The simulation was used to compute the combinatorial background. The samples were normalised using events in the side band region defined by $0.2 < \Delta M < 0.4 \text{ GeV}/c^2$. The statistical error on the normalisation factor was $\pm 2\%$ and was considered as a contribution to the systematic error. In addition a shift of $\sim 1 \text{ MeV}/c^2$ was applied to the ΔM distribution of the simulated background events to match the data in the wrong charge correlation. To account for a possible systematic error due to the lack of knowledge of the shape of the combinatorial background, the measurement was repeated with and without a corresponding shift of $1 \text{ MeV}/c^2$ of the simulated background distribution for the right charge correlated events. The difference between the results was taken as a contribution to the systematic error and added to the statistical uncertainty on the normalization factor. The result was considered as the total systematic error due to the combinatorial background subtraction procedure.

The results of sections 6 and 7 were used to determine the uncertainty on the total amount of physics background.

The corresponding variations on the branching ratio and on $|V_{cb}|$ were included in the systematic error.

Errors due to the parameterisation of the resolution function and to the details of the fit procedure affect only the values of $|V_{cb}|$ and a^2 . They were estimated by varying the bin size and the values of the parameters within the ranges allowed by the simulation. The effect on $|V_{cb}|$ was $\pm 3.0\%$. To test that the resolution function was correctly described by the simulation, the fit was performed either including or excluding events which, due to the finite resolution, lay at $q^2 < 0 \text{ GeV}^2/c^4$. About 30% of events were removed in this way. The fit was then computed by removing events with $q^2 > 9 \text{ GeV}^2/c^4$. The total variation on $|V_{cb}|$ was $\pm 1.2\%$. By summing the two last sources of uncertainty a total systematic error of $\pm 3.2\%$ was obtained.

10 Combined result

The $Br(B^0 \rightarrow D^{*-} \ell^+ \nu)$ branching fractions measured in the exclusive and inclusive analysis were respectively:

$$\begin{aligned} Br(B^0 \rightarrow D^{*-} \ell^+ \nu) &= (4.91 \pm 0.45(\text{stat}) \pm 0.77(\text{syst}))\% \\ Br(B^0 \rightarrow D^{*-} \ell^+ \nu) &= (5.65 \pm 0.17(\text{stat})_{-0.74}^{+0.68}(\text{syst}))\%. \end{aligned}$$

From the fit to the measured q^2 spectrum the following results were obtained for the exclusive analysis:

$$\begin{aligned} F(q_{max}^2)|V_{cb}| &= (34.2 \pm 3.4(\text{stat}) \pm 2.9(\text{syst})) \cdot 10^{-3} \\ a^2 &= 0.77 \pm 0.26(\text{stat}) \pm 0.10(\text{syst}), \end{aligned}$$

and for the inclusive analysis:

$$\begin{aligned} F(q_{max}^2)|V_{cb}| &= (35.9 \pm 2.2(\text{stat}) \pm 2.5(\text{syst})) \cdot 10^{-3} \\ a^2 &= 0.74 \pm 0.20(\text{stat})_{-0.16}^{+0.18}(\text{syst}). \end{aligned}$$

In combining the results from the two samples the correlation between systematic errors was taken into account. The systematic effects due to the imprecise knowledge of the $D^{*-} \ell^+$ reconstruction efficiency and of the q^2 resolution were considered uncorrelated since the experimental procedure to extract the signal was different in the two analyses. The other contributions were taken to be correlated. The statistical correlation between the two samples was estimated to be 5%. Averaging the measurements gave the following results:

$$\begin{aligned} Br(B^0 \rightarrow D^{*-} \ell^+ \nu) &= (5.52 \pm 0.17(\text{stat}) \pm 0.68(\text{syst}))\% \\ F(q_{max}^2)|V_{cb}| &= (35.4 \pm 1.9(\text{stat}) \pm 2.4(\text{syst})) \cdot 10^{-3} \\ a^2 &= 0.75 \pm 0.17 \pm 0.10 \end{aligned}$$

with a confidence level of 0.48 and 0.76 on the first two averages. In both cases the dominant systematic is the uncertainty in the D^{**} contribution.

Using the value $F(q_{max}^2) = 0.91 \pm 0.04$ [7] gave the following value for $|V_{cb}|$:

$$|V_{cb}| = (38.9 \pm 2.0(\text{stat}) \pm 2.6(\text{syst}) \pm 1.7(\text{theory})) \cdot 10^{-3}.$$

11 Conclusion

A search for events containing in the same hemisphere an exclusively reconstructed $D^{*-} \ell^+$ pair and a secondary pion of charge opposite to the D^{*-} was performed using the data sample collected by the DELPHI detector in 1994. The ratio:

$$\begin{aligned} &\frac{Br(B \rightarrow D^{*-} \ell^+ \nu X)}{Br(B \rightarrow D^{*-} \ell^+ \nu X) + Br(B^0 \rightarrow D^{*-} \ell^+ \nu)} \\ &= 0.19 \pm 0.10(\text{stat}) \pm 0.06(\text{syst}) \end{aligned}$$

was measured.

The q^2 distributions of samples of exclusively and inclusively reconstructed $D^* \ell$ were studied. From fits to these distributions, the product of $|V_{cb}|$ times the normalization of the form factor $F(q_{max}^2)$ was extracted:

$$F(q_{max}^2)|V_{cb}| = (35.4 \pm 1.9(\text{stat}) \pm 2.4(\text{syst})) \cdot 10^{-3}.$$

Using the value $F(q_{max}^2) = 0.91 \pm 0.04$ [7] gave the following value for $|V_{cb}|$:

$$|V_{cb}| = (38.9 \pm 2.0(\text{stat}) \pm 2.6(\text{syst}) \pm 1.7(\text{theory})) \cdot 10^{-3}.$$

The total branching fraction $Br(B^0 \rightarrow D^{*-} \ell^+ \nu)$ was determined to be

$$Br(B^0 \rightarrow D^{*-} \ell^+ \nu) = (5.52 \pm 0.17(\text{stat}) \pm 0.68(\text{syst}))\%.$$

These results are consistent with the most precise previous measurements [9, 11] and are of comparable precision. The use of both inclusive and exclusive methods of D^* reconstruction has resulted in the smallest statistical error on $F(q_{max}^2)|V_{cb}|$ and on the branching ratio $Br(B^0 \rightarrow D^{*-} \ell^+ \nu)$.

Acknowledgements. We are greatly indebted to our technical collaborators and to the funding agencies for their support in building and operating the DELPHI detector, and to the members of the CERN-SL Division for the excellent performance of the LEP collider.

References

1. Particle Data Group, "Review of Particle Properties", Phys. Rev. **D50**, Part I (1994).
2. M. Neubert, Phys. Lett. **B264** (1991) 455;
3. N. Isgur and M. Wise, Phys. Lett. **B 232** (1989) 113.
4. A. Falk, M. Neubert and M. Luke, Nucl. Phys. **B 388** (1992) 3362; A.F. Falk and M. Neubert, Phys. Rev. **D 47** (1993) 2965; M. Neubert, Phys. Rev. **D 47** (1993) 4063.
5. M.E. Luke, Phys. Lett. **B 252** (1990) 447.
6. M. Neubert, Phys. Lett. **B 338** (1994) 84.
7. M. Neubert, "Uncertainties in the determination of $|V_{cb}|$ ", preprint CERN-TH/95-107 (1995), hep-ph/9505238.
8. H. Albrecht et al., ARGUS Collab., Z. Phys. **C 57** (1993) 533;
9. B. Barish et al., CLEO Collab., Phys. Rev. **D51** (1995) 1014.
10. D. Buskulic et al., ALEPH Collab., Phys. Lett. **B 359** (1995) 236
11. D. Buskulic et al., ALEPH Collab., Phys. Lett. **B 345** (1994) 103; R. Akers et al., OPAL Collab., Zeit. Phys. **C67** (1995) 57.
12. P. Aarnio et al., DELPHI Collab., Nucl. Instr. & Meth. **A 303** (1991) 233.
13. P. Abreu et al., DELPHI Collab., "Performance of the Delphi Detector", CERN-PPE/95-154, submitted to Nucl. Instr. & Meth. A.
14. V. Chabaud et al., DELPHI Collab., Nucl. Instr. & Meth. **A 368** (1996) 314.

15. T. Sjöstrand: *Comp. Phys. Comm.* **39** (1986) 347;
- T. Sjöstrand and M. Bengtsson: *Comp. Phys. Comm.* **43** (1987) 367;
- T. Sjöstrand: *JETSET 7.3 manual*, CERN-TH 6488/92 (1992).
16. DELSIM Reference Manual, DELPHI 87-98 PROG 100, Geneva, July 1989.
17. P. Abreu et al., DELPHI Collab., *Zeit. Phys.* **C57** (1993) 181.
18. D. Buskulic et al., ALEPH Collab., *Phys. Lett.* **B 322** (1994) 275.
19. H. Albrecht et al., ARGUS Collab., *Phys. Letters* **B 324** (1994) 249.
20. D. Bloch et al., DELPHI Collab., "Study of Charm Mesons Production in Z Decays and Measurement of Γ_c/Γ_h ", contribution eps0557 to the International Europhysics Conference on High Energy Physics, Brussels, July 27 - August 2, 1995.
21. P. Abreu et al, DELPHI Collab., *Zeit. Phys.* **C65** (1995) 599.
22. P. Abreu et al, DELPHI Collab., *Phys. Lett.* **B 345** (1994) 598.
23. S. Komamiya, Proc. of the International Europhysics Conference on High Energy Physics, Brussels, July 27 - August 2, 1995.
24. A. Olshevski, Proc. of the International Europhysics Conference on High Energy Physics, Brussels, July 27 - August 2, 1995.
25. P. S. Wells, Proc. of the International Europhysics Conference on High Energy Physics, Brussels, July 27 - August 2, 1995.
26. P. Abreu et al., DELPHI Collab., *Zeit. Phys.* **C69** (1996) 561.
27. D. Buskulic et al., ALEPH Collab., *Phys. Lett.* **B 343** (1995) 444.
28. P. Abreu et al., DELPHI Collab., *Zeit. Phys.* **C 66** (1995) 323.